Eurasian Journal of Physics and Functional Materials

Synthesis, X-ray phase analysis and differential thermal analysis of nanocrystalline superionic KxCuiss1.85S (x<0.05) copper sulfides

S. M. Sakhabayeva

M. Kh. Balapanov

K. A. Kuterbekov

R. Kh. Ishembetov

M. M. Kubenova

See next page for additional authors

Recommended Citation

Sakhabayeva, S. M.; Balapanov, M. Kh.; Kuterbekov, K. A.; Ishembetov, R. Kh.; Kubenova, M. M.; and Giniyatova, Sh. G. (2022) "Synthesis, X-ray phase analysis and differential thermal analysis of nanocrystalline superionic KxCuiss1.85S (x<0.05) copper sulfides," *Eurasian Journal of Physics and Functional Materials*: Vol. 6: No. 1, Article 7.
DOI: https://doi.org/10.32523/ejpfm.2022060107

Synthesis, X-ray phase analysis and differential thermal analysis of nanocrystalline superionic KxCuiss1.85S (x<0.05) copper sulfides

Authors

S. M. Sakhabayeva, M. Kh. Balapanov, K. A. Kuterbekov, R. Kh. Ishembetov, M. M. Kubenova, and Sh. G. Giniyatova

Synthesis, X-ray phase analysis and differential thermal analysis of nanocrystalline superionic $K_xCu_{1.85}S$ (x<0.05) copper sulfides

S.M. Sakhabayeva[*,1,2], M.Kh. Balapanov[3], K.A. Kuterbekov[1],
R.Kh. Ishembetov[3], M.M. Kubenova[1], Sh.G. Giniyatova[1],
S.A. Nurkenov[2], B.M. Akhmetgaliev[3], M.Kh. Zeleev [4],
R.A. Yakshibaev[3], G.S. Seisenbayeva[1]

[1]L.N. Gumilyov Eurasian National University, Nur-Sultan, Kazakhstan

[2]Astana international university, Nur-Sultan, Kazakhstan

[3]Bashkir State University, Ufa, Russia

[4]Bashkir State Medical University, Ufa, Russia

E-mail: s.sakhabayeva@gmail.com

Superionic semiconductor chalcogenides with mixed electronic-ionic conductivity have very low lattice thermal conductivity and are excellent thermoelectrics. Doping with other elements is one of the methods for optimizing the useful properties of a material. In this work, nanosized polycrystalline alloys of nonstoichiometric $Cu_{1.85}S$ copper sulfide with a low content of potassium are studied. The paper presents the results of X-ray phase analysis, differential thermal analysis (DTA) and electron microscopy of differential thermal analysis of $K_xCu_{1.85}S$ alloys. The resulting alloys are a mixture of phases, in which the main share is djurleite - non-stoichiometric copper sulfide of the composition $Cu_{1.97\div1.93}S$, in addition, depending on the composition of the alloy, there are impurities of monoclinic and hexagonal chalcocite Cu_2S, roxbyite $Cu_{1.81}S$, anilite $Cu_{1.75}S$, traces of metallic copper. All alloys contain inclusions of Cu_2O copper oxide. DTA detected a superionic phase transition from an ordered low-symmetry djurleite phase to a disordered superionic hexagonal phase of copper sulfide at about 373-383 K. In addition, DTA revealed two thermal effects at about 433 K and 460 K, which are absent in binary copper sulfide. The reason for the effects may be the redistribution of impurity potassium ions in the copper sulfide lattice.

Keywords: nanocrystalline copper sulfides; X-ray phase analysis; differential thermal analysis; djurleite; superionic chalcogenides; phase transition

Introduction

Superionic semiconductor materials with mixed electronic-ionic conductivity have very low lattice thermal conductivity and are excellent thermoelectrics. Doping with other elements is one of the methods for optimizing the useful properties of a material [1-5].

There are several works on doping copper chalcogenides with potassium. The paper [6] describes the results of measurements of electronic conductivity and Seebeck coefficient, thermal conductivity coefficient of stoichiometric alloys $K_xCu_{2-x}S$ (x=0.1, 0.2, 0.25) in the temperature range from 30 to $420°C$. According to the results of X-ray phase analysis, the alloys were a mixture of different copper sulfide phases: cubic $Cu_{1.84}S$ phase, cubic Cu_2S phase, rhombohedral $Cu_{17}S_9$ phase, and metastable tetragonal Cu_2S phase. Differential scanning calorimetry revealed an endothermic peak, extended from 84 to $102°C$, caused by phase transitions from the rhombohedral and tetragonal phases to the hexagonal phase of copper sulfide. In the temperature range above room temperature, for all samples, a semiconductor character of conductivity is observed, which then changes to metallic (above $102°C$, $93°C$ and $270°C$ for alloys $K_{0.1}Cu_{1.9}S$, $K_{0.2}Cu_{1.8}S$, $K_{0.25}Cu_{1.75}S$, respectively). The conduction activation energy is 0.16, 0.22, and 0.39 eV for $K_{0.1}Cu_{1.9}S$, $K_{0.2}Cu_{1.8}S$, $K_{0.25}Cu_{1.75}S$, respectively. In the range from 130 to $270°C$, the activation energy of the $K_{0.25}Cu_{1.75}S$ alloy decreases to 0.16 eV also. It is interesting that in the low-temperature region - up to $100°C$, the conductivity of the alloys decreases with increasing potassium content, and above $100°C$ an inversion occurs - the dependence of the conductivity on the potassium concentration becomes opposite. Even more interesting is that the Seebeck coefficient does not experience such inversion. Near $370°C$, Balapanov et al [6] observed an abrupt decrease in conductivity, a sharp increase in the Seebeck coefficient. According to the handbook by D. Chakrabarti and D. Laughlin [7], as the temperature rises, the equilibrium content of copper in cubic digenite gradually tends to Cu_2S composition: at $100°C$, the limiting copper deficiency corresponds to $Cu_{1.835}S$ composition; at $150°C$ - $Cu_{1.875}S$, at $200°C$ - $Cu_{1.902}S$, at $300°C$ - $Cu_{1.944}S$, at $435°C$ - $Cu_{1.999}S$. The hole conductivity of $Cu_{2-\delta}S$ copper sulfide is caused by cation vacancies, the concentration of which is proportional to the degree of nonstoichiometricity δ [8], therefore, when digenite $Cu_{1.84}S$, whose content in the alloy is close to half, is heated, the conductivity of the alloy decreases due to a decrease in the concentration of holes in the cubic digenite phase. According to K. Okamoto and Sh. Kawai [8], the conductivity of digenite with the composition $Cu_{1.84}S$ at $20°C$ is 2100 $Ohm^{-1}cm^{-1}$, and with a composition close to Cu_2S, the conductivity, depending on the preparation method, is $5 \div 15$ $Ohm^{-1}cm^{-1}$. Balapanov et al [6] observed a strong increase in Seebeck coefficient for the $K_{0.2}Cu_{1.8}S$ composition above $300°C$ (up to 4 mV/K) and a decrease in thermal conductivity (from 0.87 to 0.4 W/m K), leading to a very high peak value of the dimensionless thermoelectric figure of merit ZT=3.5 at $380°C$.

Sakhabayeva S.M. et al., [9] presented the study results in thermal conductivity and heat capacity of nanocrystalline copper sulfides $K_{0.01}Cu_{1.85}S$ and

$K_{0.04}Cu_{1.85}S$ at the temperature range between 27 and 427°C. For both samples, an endothermic thermal effect is observed near 417°C. In copper sulfide at 437°C, the phase transition occurs from the hexagonal to the cubic Cu_2S phase [10], and it is known that the lack of copper in the lattice reduces the phase transition temperature. So, the observed thermal effect near 417°C authors of work [9] conclude to be caused by this phase transition. In the investigated temperature range the Zeebeck coefficient α for $K_{0.04}Cu_{1.85}S$ increase to reaching a pick of 1.96 mV/K, before falling to around 0.32 mV/K. For the studied alloys, a strong contrast in electronic conductivity in both components of the alloy was observed and a dramatic decrease in thermal conductivity (from 2.0 to 0.5 W m^{-1} K^{-1}), leading to extremely high local peak value of the dimensionless thermoelectric figure of merit ZT=9.67 at 347°C, which is important for possible technical applications.

Li X. [11] reported about $KCu_{7-x}S_4$ nanowires, which demonstrate enhanced thermoelectric properties compared to binary Cu_7S_4 nanocrystals. The presence of K^+ ions forms a clathrate and superionic liquid structure, which provides the state of "phonon glass" and "liquid-electronic crystal". Low thermal conductivity (less than 0.5 W $m^{-1}K^{-1}$ in the range of 52-302°C) and a large Seebeck coefficient (0.1 ÷ 0.19 mV/K in the range 152-302°C) were observed when nanowires were pressed into a bulk material. Pressed plates from $KCu_{7-x}S_4$ nanowires showed peak values of thermoelectric figure of merit $ZT \approx 0.12$ at 77°C, $ZT \approx 0.19$ at 302°C [11].

Balapanov et al., [12] performed investigations of nanocrystalline $K_xCu_{1.97-y}S$ (0<x<0.05, y<0.03) copper sulfides. X-ray phase analysis at room temperature showed that the samples are mixtures of various phases of the copper sulfide. The composition of $K_{0.01}Cu_{1.96}S$ includes the phases $Cu_{1.97}S$ (monoclinic djurleite), Cu_2S (monoclinic chalcocite), and there are traces of the cubic phase of Cu_2O oxide. Alloy $K_{0.05}Cu_{1.94}S$ consists from tetragonal djurleite $Cu_{1.96}S$ and monoclinic chalcocite (Cu_2S). The crystallite sizes calculated from the half-width of X-ray lines are in the range 10-64 nm for $K_{0.01}Cu_{1.96}S$ and 7-47 nm for $K_{0.05}Cu_{1.94}S$. The results of differential scanning calorimetry and temperature dependences of Seebeck coefficient are presented in the range of 30-427°C. A strong thermal effect of about 105°C is observed in all samples, which corresponds to a high content of the monoclinic chalcocite phase in the alloys. On the DSC curves of all alloys there is also an endothermic thermal effect in the range of 449-470°C. High values of Seebeck coefficient are observed from 0.17 to 0.72 mV/K in the temperature range 30-200°C, which will be useful for possible thermoelectric applications.

Potassium doping in copper selenide was studied by Z. Zhu et al., [13] using the hydrothermal synthesis and hot pressing. The nanopowders of K-doped Cu_2Se were synthesized using pure $CuCl_2 \cdot 2H_2O$, KF and SeO_2 powder as precursors. Numerous micro-pores were introduced by K doping, together with reduced electronic conductivity that result in low thermal conductivity. It was observed that the density of the micro-pore in the materials increases with the increasing K content. As the number of micro-pores increases, the relative density of samples decreases gradually from 96.2 to 91.8%. The relative theoretical

densities of the samples are 96.2%, 95.3%, 93.5%, and 91.8% for the x=0, 0.01, 0.02, and 0.03 samples, respectively. The mechanism of introducing micro-pore structure in K-doped samples is still a problem to be solved. We note that similar effects were found in other copper chalcogenides at doping by Na too [14, 15]. For the nominal component $Cu_{1.97}K_{0.03}Se$ (EPMA measured composition $Cu_{1.99}K_{0.01}Se$), the peak value of ZT reaches 1.19 at $500°C$, which is 47% larger than that of pure Cu_2Se (ZT_{max} =0.81).

In the work [16] copper sulfide (Cu_2S) nanocrystals and K or Na doped KCu_7S_4 nanowires and $NaCu_5S_3$ micro-nanospheres have been synthesized successfully by using a simple hydrothermal method, using KOH or NaOH as mineralizing agent, $CuCl_2 \cdot 2H_2O$ and S powders as copper and sulfur sources, respectively. The results reveal that under conditions that the amount of KOH is below 1g or the amount of NaOH below 2 g, the product is of the orthorhombic chalcocite Cu_2S, while with high alkali amount (no less than 3 g), K^+ or Na^+ is successfully incorporated into the Cu-S structure; KCu_7S_4 has the pure tetragonal single crystal structure, and its uniform nanowires can be up to several tens of micrometers in length. Na doping has no effect on the morphology of the product, which forms the hexagonal $NaCu_5S_3$. The formation and growth of the product are closely related to the reaction temperature, reaction time and mineralizing agent. The diffuse reflectance spectra demonstrate that the optical band gaps of Cu_2S, $NaCu_5S_3$ and KCu_7S_4 nanocrystallines is 1.21, 0.49, 0.42 eV, respectively.

Currently, a significant amount of research is being performed in the synthesis of nanostructured materials, however, in order for the material to be practical for a real thermoelectric device, it must be combined into a compacted bulk granule.

Materials with low density usually have poor mechanical properties and are difficult to work with. Numerous porosity studies show that electrical properties can deteriorate by orders of magnitude when the sample does not have a full theoretical density [17]. This is due to additional charge scattering and violation of the free path of the electron as it moves from one sample to another grain to another. It was also found that porosity affects the results of thermal conductivity [18]. The total thermal conductivity, κ, is the product of the thermal conductivity α, the heat capacity C_p and the density ρ (equation (1).

$$\kappa = \alpha \rho C_p, \qquad (1)$$

Since one of the parameters of thermal conductivity is density, a low-density material will inherently have low thermal conductivity. In addition, the pores can act as phonon scattering sites, thereby reducing the thermal conductivity of the lattice. Theoretically, the ideal nanostructured inclusion for reducing thermal conductivity is a nanoscale void, however, in order for the void to be an effective phonon diffuser, it must be on the order of several nanometers [19]. Therefore, when studying the effect of nanostructuring on thermoelectric properties, it is extremely important that the materials being evaluated have the same high density.

There are three main methods that are commonly used for compacting nanostructured materials: cold pressing followed by sintering, hot uniaxial pressing

(hot pressing) and spark plasma sintering (SPS). A relatively new method that can be used to sinter "softer" materials is known as compaction by burning.

Cold pressing

During cold pressing followed by sintering, the materials are loaded into a mold (usually stainless steel) and hydrostatic pressures of about 5 tons are applied, usually using a Carver press. The granules are then extracted and heated to about 70% of the theoretical melting point for sintering the nanopowder. If everything is done correctly, it is possible to obtain samples with a density of up to 90 percent of the theoretical [20].

Hot pressing

In the hot-pressing method, the material is first loaded into a graphite matrix, and then into a press [21]. Pressure is applied in one direction while the sample is heated to about 70% of its theoretical melting point by heating graphite or ceramics Elements [22, 23]. The compact density usually reaches 95-100% of the theoretical density [24, 25]. This sealing method can be used for various materials.

Spark plasma sintering

The method associated with hot pressing is spark plasma sintering (SPS). There are various names for this process, but the main technology differs from hot pressing in that a pulsed direct current is passed through graphite dies under hydrostatic uniaxial pressure. As a result, high temperatures are reached relatively quickly (minutes, not hours in most hot presses) [26, 27]. Extracted granules can have a density approaching 95-100% of the theoretical density. It is believed that since SPS requires a relatively short sintering time, this can prevent the grain enlargement of nanoparticles, effectively keeping them small [28]. However, this has yet to be seen experimentally.

Perhaps the most important test of bulk nanostructured thermoelectric materials is their long-term thermal stability. Thermal stability is a key aspect of a nanostructured thermoelectric device, because for practical applications, thermoelectric devices must operate for extended periods of time, often more than 10-15 years. There is no advantage in the synthesis of nanostructured bulk materials if nanoscale elements are combined back into coarse-grained bulk materials or stratified into composites at the macro level.

In our work a cold pressing was used for nanostructured material compacting.

The work presents results of synthesis of nanostuctured chalcogenide thermoelectric materials with a poor potassium content.

The optimal technology for the synthesis of thermoelectric superionic materials depends on the synthesis goals. The synthesis of a new chalcogenide material in small quantities for the study of thermoelectric and other properties is advisable to be carried out by direct solid-phase reaction in vacuum or in an atmosphere of purified inert gas. This method is more reliable, allows to get a pure product that does not contain impurities that are inevitable when using various solvents and precursors. In addition, it is characterized by the stability of the properties of the resulting compounds while maintaining a constant synthesis mode. By increasing the synthesis temperature to the melting point, it is possible to increase the density of the resulting material to the maximum, which is important for thermoelectric applications. Synthesis modes, reagents, and subsequent

processing depend on the specific material.

In the synthesis of thermoelectric material, the properties of which are known for commercial purposes, the main task is to achieve the cheapness of products while maintaining the useful properties obtained in laboratory studies. Recently, almost all leading laboratories developing thermoelectric materials have been using methods of "soft" chemistry that allow synthesis at low temperatures, ideally close to room temperatures, since it is believed that this reduces production costs.

Within the framework of this work, a method for the synthesis of alloys in a melt medium of a mixture of potassium and sodium hydroxides has been developed. At a certain ratio of concentrations of these hydroxides, the melting point decreases to $165°C$, which allows exchange reactions between salts in the melt. Reducing the synthesis temperature and reducing the annealing time makes it possible to reduce the size of the resulting chalcogenide particles to units of nanometers.

Materials and methods

The synthesis reaction is carried out in a melt of NaOH and KOH hydroxides. It is known that the melting point of pure NaOH is $323°C$, for KOH the melting point is $400°C$. With a quantitative ratio between NaOH/KOH=51.5:48.5, the melting point of the mixture decreases to $165°C$.

Initially, the prepared mixture of sodium and potassium hydroxides in the ratio is placed in a Teflon vessel and heated to melting (approximately $165°C$).

All reagents (CuCl, KCl, $Na_2S \cdot 9H_2O$) are placed in a heated Teflon vessel simultaneously. After laying the charge, the vessel is filled with argon and tightly closed with a threaded lid. In the first half hour, mixing of the solution is recommended, which can be replaced by vibration or shaking.

The $K_xCu_{1.85}S$ nanostructure is formed within a few hours, usually a time of 15 hours is maintained. The sizes of nanocrystallites can be varied by adding a small amount of water to the melt. The product obtained in the form of a clot was washed three times with heated distilled water, then washed with pure ethanol and dried at room temperature.

The sizes of nanocrystallites were estimated from half-width of X-ray diffraction lines. A particle size distribution within 30-150 nm was observed.

X-ray diffraction analysis (XRD, Cu $K\alpha$, Bruker D8, Germany) was used to study the phase composition of alloys. The X-rays used in the XPS measurements were obtained by a monochromatized Al anode (Al $K\alpha$ =1486.6 eV). Before XPS measurement, the samples were spray cleaned for 30 seconds with an Ar^+ ion beam (4 kV, 10 mA) in vacuum to remove surface contaminants.

Results and Discussion

X-ray phase analysis

Figure 1 demonstrates the X-ray powder diffraction patterns of the nanocrystalline copper sulfide alloys $K_xCu_{1.85}S$ (0<x<0.05) taken at room temperature.

The results of the X-ray phase analysis are presented in Table 1.

Potassium seems to be dissolved in the voids of the copper sulfide crystal lattice, since apart from various phases of copper sulfide, no potassium-containing phases were found.
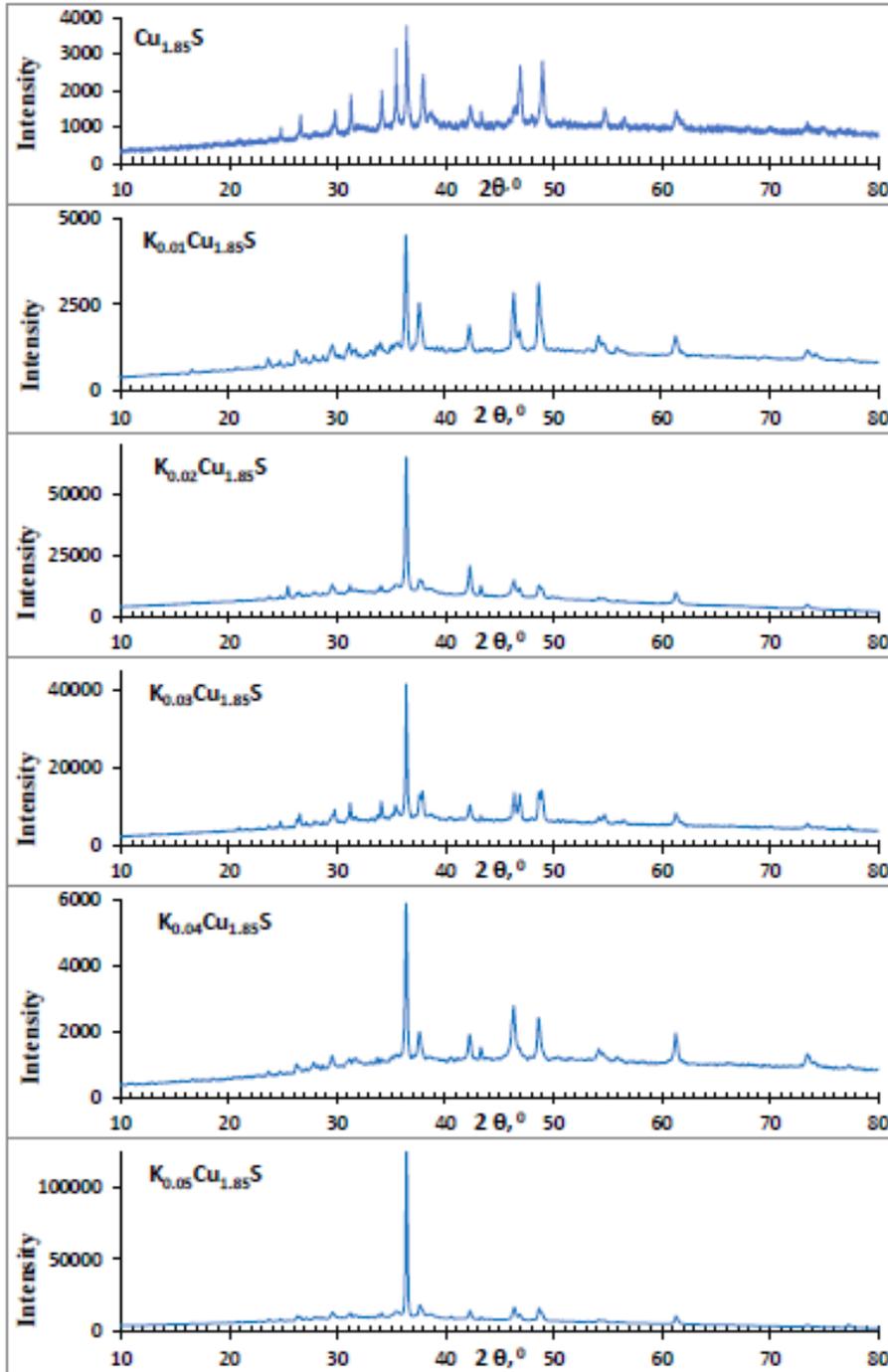

Figure 1. Powder diffraction patterns of samples $K_xCu_{1.85}S$ (x=0.01, 0.02, 0.03, 0.04, 0.05) received at room temperature.

It can be seen in Table 1 that the $Cu_{31}S_{16}$ (or $Cu_{1.9375}S$) monoclinic djurleite phase are found as prevailing in all $K_xCu_{1.85}S$ samples (0.01<x<0.05). Also in all samples there are oxygen oxide Cu_2O and orthorhombic anilite $Cu_{1.75}S$. Variable components of the alloys are monoclinic and hexagonal chalcocite, roxbyite. Appearance of a hexagonal chalcocite at room temperature may be

Table 1.
Results of X-ray phase analysis of the $K_xCu_{1.85}S$ samples (x=0.01, 0.02, 0.03, 0.04, 0.05) at room temperature.

Phase	Phase name	Crystal System:	Space Group	Z	Volume, Å³	Cell, Å,°	Phase content in sample
					$Cu_{1.85}S$		
$Cu_{29}S_{16}$	Roxbyite	Triclinic	P-1(2)	4	2783.448	13.4090, 13.4051, 15.4852, 90.022, 90.021, 90.020 [29]	70%
Cu_2O	Copper oxide (I)	cubic	Pn3m (224)	2	77.833	4.2696 [30]	14%
Cu_7S_4	Anilite	Orthorhombic	Pnma(62)	4	685.141	7.8900, 7.8400, 11.0100, 90.000, 90.000, 90.000 [31]	16%
					$K_{0.01}Cu_{1.85}S$		
$Cu_{31}S_{16}$	Djurleite	Monoclinic	P21/n(14)	8	5702.322	26.8970, 15.7450, 13.4650, 90.000, 90.130, 90.000 [32]	70%
Cu_2O	Copper oxide (I)	cubic	Pn3m (224)	2	77.833	4.2696	15%
Cu_7S_4	Anilite	Orthorhombic	Pnma(62)	4	685.141	7.8900, 7.8400, 11.0100, 90.000, 90.000, 90.000	9%
Cu_2S	Chalcocite	Hexagonal	P63/mmc (194)	2	91.335	3.959(2), 6.784(4) [33]	6%
					$K_{0.02}Cu_{1.85}S$		
$Cu_{31}S_{16}$	Djurleite	Monoclinic	P21/n(14)	8	5702.322,	26.8970, 15.7450, 13.4650, 90.130, 90.000, 90.000,	63%
Cu_2O	Copper oxide (I)	cubic	Pn3m (224)	2	77.833	4.2696	17%
$Cu_{29}S_{16}$	Roxbyite	Triclinic	P-1(2)	4	2783.448	13.4090, 13.4051, 15.4852, 90.022, 90.021, 90.020	8%
Cu_2S	Chalcocite	Monoclinic	P21/c (14)	48	2190.864	15.2460, 11.8840, 13.4940, 90.000, 116.350, 90.000 [34, 35]	5%
Cu_7S_4	Anilite	Orthorhombic	Pnma(62)	4	685.141	7.8900, 7.8400, 11.0100, 90.000, 90.000, 90.000	7%

Phase	Phase name	Crystal System:	Space Group	Z	Volume, Å³	Cell, Å,°	Phase content in sample
					$K_{0.03}Cu_{1.85}S$		
$Cu_{31}S_{16}$	Djurleite	Monoclinic	P21/n(14)	8	5702.322	26.8970, 15.7450, 13.4650, 90.000, 90.130, 90.000	68%
Cu_2O	Copper oxide (I)	cubic	Pn3m (224)	2	77.833	4.2696	16%
$Cu_{29}S_{16}$	Roxbyite	Triclinic	P-1(2)	4	2783.448	13.4090, 13.4051, 15.4852, 90.022, 90.021, 90.020	7%
Cu_7S_4	Anilite	Orthorhombic	Pnma(62)	4	685.141	7.8900, 7.8400, 11.0100, 90.000, 90.000, 90.000	9%
					$K_{0.04}Cu_{1.85}S$		
$Cu_{31}S_{16}$	Djurleite	Monoclinic	P21/n(14)	8	5702.322	26.8970, 15.7450, 13.4650, 90.000, 90.130, 90.000	74%
Cu_2O	Copper oxide (I)	cubic	Pn3m (224)	2	77.833	4.2696	15%
Cu_2S	Chalcocite	Monoclinic	P21/c (14)	48	2190.864	15.2460, 11.8840, 13.4940, 90.000, 116.350, 90.000	7%
Cu_7S_4	Anilite	Orthorhombic	Pnma(62)	4	685.141	7.8900, 7.8400, 11.0100, 90.000, 90.000, 90.000	4%
					$K_{0.05}Cu_{1.85}S$		
$Cu_{31}S_{16}$	Djurleite	Monoclinic	P21/n (14)	8	5702.322	26.8970, 15.7450, 13.5650, 90.000, 90.130, 90.000	77%
Cu_2O	Copper oxide (I)	Cubic	Pn3m (224)	2	77.833	4.2696	19%
Cu_7S_4	Anilite	Orthorhombic	Pnma(62)	4	685.141	7.8900, 7.8400, 11.0100, 90.000, 90.000, 90.000	4%

caused by insertion of potassium into crystal lattice of low (monoclinic) chalcocite, which leads to the structural transformation. We note that in binary $Cu_{1.85}S$ sample the hexagonal chalcocite phase is absent (Table 1).

Differential thermal analysis

Figure 2 shows the results of differential thermal analysis for all $K_xCu_{1.85}S$ samples (x=0.01, 0.02, 0.03, 0.04, 0.05). The first endothermic peak is observed at about $60°C$ for all compositions, except $K_{0.03}Cu_{1.85}S$, in which it is shifted to $67°C$. The effect is weak for $K_{0.05}Cu_{1.85}S$ and $K_{0.02}Cu_{1.85}S$; for the rest, it is quite pronounced.

Authors of paper [36] presented an investigation of the size-dependent, temperature-induced solid-solid phase transition in copper sulfide nanorods from low- to high-chalcocite. Length of nanorods not affects to temperature of the phase transition, but diameter of nanorods affects greatly. At 4 nm nanorod diameter the phase transition is observed at $52\text{-}62°C$. Twinning in nanocrystals can enhance the effect of temperature reduction. A recent work by J. Gong and P.K. Jain [37] describes the preparation of $Cu_{1.93}S$ nanocrystals with the superionic phase transition temperature from 72 to $0°C$. Single-domain $Cu_{1.97}S$ nanocrystals were about 7 nm in size and had a temperature $T_c \approx 74°C$, whereas in the bulk, the temperature for such a transition is $\approx 104°C$ (for chalcocite) and $97°C$ (for djurleite) [7].

The lower T_c for the NCs is due to the nanoscale size effect, which is known to result in a depression in phase transition temperature [36]. The average domain size (3.8 nm) of multi-domain $Cu_{1.93}S$ NCs is appreciably smaller than the average NC diameter (7.2 nm). At the high temperature (in our case it is $165°C$) at which the synthesis by J. Gong is performed, the NCs are formed with a high-temperature hexagonal arrangement of S_2^-.Cooling imposes a transition from this higher-symmetry hexagonal form to the lower symmetry monoclinic form. The lost symmetry element instead becomes a twin law: the monoclinic lattice formed is non-merohedrally twinned such that it adopts a hexagonal supercell [38]. This explains why NCs synthesized with the djurleite composition undergo twinning.

The relative depression in the T_c for a twinned NC with respect to the bulk value (i.e., T_c^{bulk}) is given as:

$$\frac{T_C^{bulk} - T_C^{TNC}}{T_C^{bulk}} = \left(\frac{\zeta_S A_S}{\rho V \Delta H^{bulk}} + \frac{\zeta_{TB} A_{TB}}{\rho V \Delta H^{bulk}}\right), \tag{2}$$

The first term on the right-hand side represents the depression caused by the nanoscale size. The smaller the NC size, the higher the surface area-to-volume ratio (As/V) and the larger is this contribution. The second term on the right-hand side represents the additional depression caused by the presence of twin boundaries. Higher the density of twin boundaries (ATB/V), greater is this depression. This simple model thus explains the reduction in the Tc caused by the presence of twinning. So, this double effect may be caution of the first thermal effect in our Figure 2, and we see the phase transition from low (monoclinic) djurleite to hexagonal chalcocite at $60°C$. The proportion of nanocrystallites less than 7 nm in the alloy is small, the size distribution of nanocrystallites is quite

wide and smooth, which leads to a corresponding distribution of Tc values, so we observe a small blurred peak at about 60°C in Figure 2.

For the main phase of our alloys - monoclinic djurleite, the phase transition to its hexagonal modification occurs in coarse-grained materials at about 97°C according to Chakrabarti [7]. We see this transition as a pronounced endothermic effect in Figure 2 at 98.7°C for $K_{0.01}Cu_{1.85}S$ and at 99.6°C for $K_{0.04}Cu_{1.85}S$. A similar but weaker thermal effect is observed at a temperature of about 97°C for the $K_{0.03}Cu_{1.85}S$ sample.
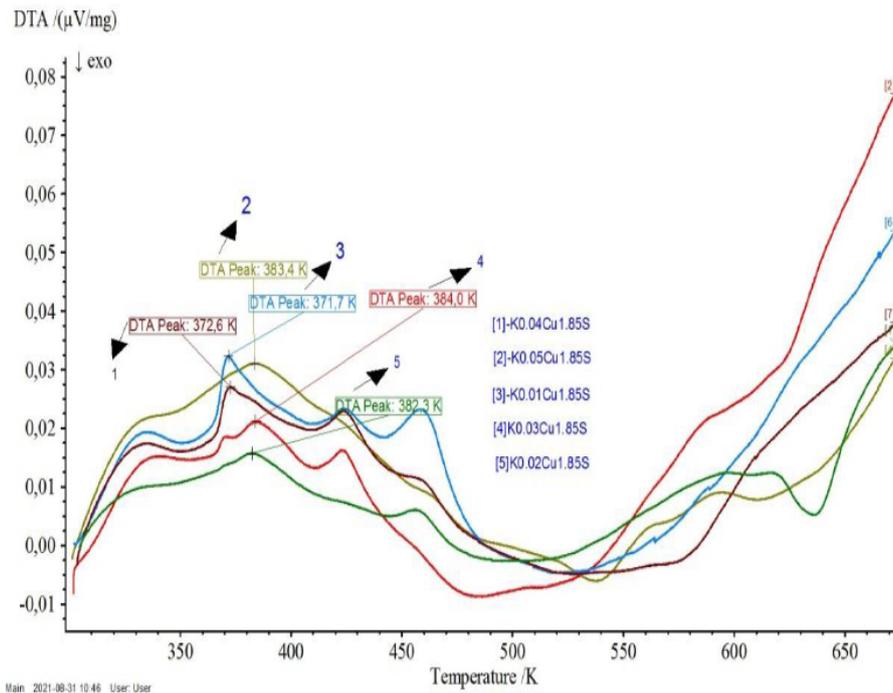
Figure 2. The DTA curves of $K_xCu_{1.85}S$ samples (x=0.01, 0.02, 0.03, 0.04, 0.05).

For three alloys ($K_{0.05}Cu_{1.85}S$, $K_{0.03}Cu_{1.85}S$, $K_{0.02}Cu_{1.85}S$), we see in Figure 2 this thermal effect shifted to $109\text{-}111^\circ$C, the shape of the peak became flat. Obviously, the reason for this is potassium, which entered the jarleite lattice. For two samples - $K_{0.03}Cu_{1.85}S$, $K_{0.04}Cu_{1.85}S$ - an endothermic peak is observed at about 150°C, for two other samples - $K_{0.01}Cu_{1.85}S$, $K_{0.02}Cu_{1.85}S$ - there is an endothermic effect at about $187\text{-}190^\circ$C. For $K_{0.04}Cu_{1.85}S$, both of these effects take place. The reason for these effects is unclear and needs to be investigated. It is possible that the existing individual phases are fused into new phases. For known modifications of copper sulfide, there are no references in the literature to phase transitions in this temperature range. With further heating to 400°C, no more thermal effects were noted in Figure 2, except for the exothermic effect at about 362°C for $K_{0.02}Cu_{1.85}S$. In the work [9] an endothermic thermal effect is observed near 417°C for $K_{0.01}Cu_{1.85}S$ and $K_{0.04}Cu_{1.85}S$, which is obviously caused by the transition from the hexagonal phase of copper sulfide to the cubic phase.

Electron microscopy

Figure 3 shows image of a transmission electron microscope (TEM) and a high-resolution transmission electron microscope (TEM) of $K_{0.02}Cu_{1.85}S$. In the

low magnification mode, the powder $K_{0.02}Cu_{1.85}S$ is uniformly dispersed on the support membrane of the microlattice, have a particle size of 8.4 mm. This very small particle size obtained directly by the synthesis method is common. Nanopowder $K_{0.02}Cu_{1.85}S$ was then compacted to a volumetric form by cold pressing. In the lower images of Figure 3 one can see a non-uniform distribution of oxygen and sulfur over the surface and rather large pores are noticeable. Copper is more evenly distributed. This confirms the conclusions of X-ray analysis, according to which the alloys consist of copper oxide and various forms of copper sulfide.
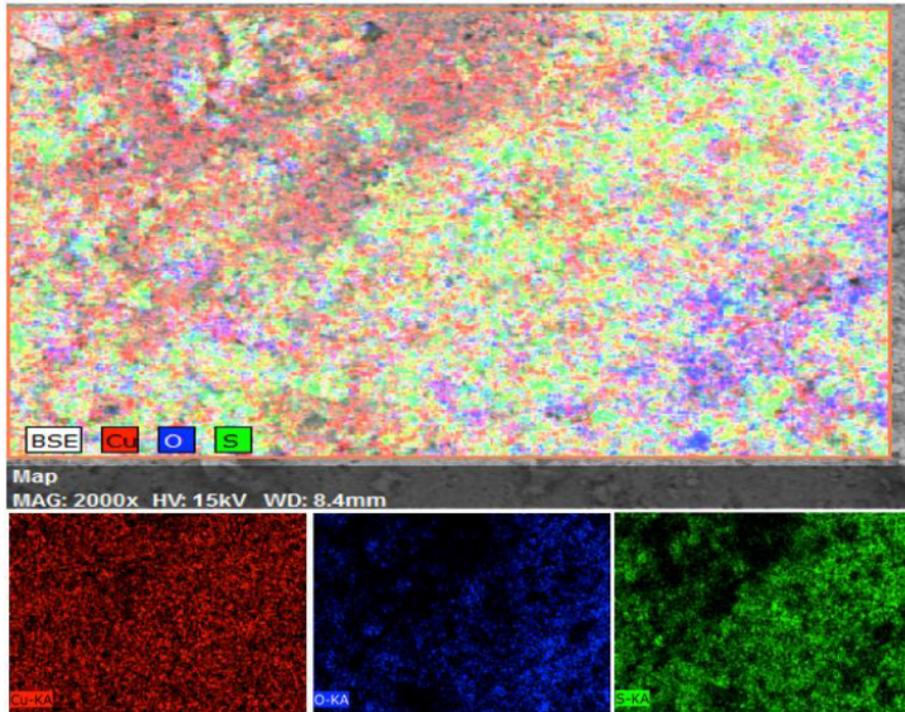

Figure 3. TEM image confirms particle size distribution.

Figure 4 shows the high density of dark contrast nanostructures in bulk materials $K_{0.02}Cu_{1.85}S$. The results of energy dispersive X-ray spectroscopy (ERS) confirmed that the dark areas in the dark field image (box in Figure 3) are pores due to the similar composition between the dark areas and the white areas. The pore size ranges from 5 to 40 nm. Many TEM studies in a wide region have shown that nanoscale grains and nanopores are located separately, that is, usually we can only see one type of nanostructure, either nanoscale grains or nanopores in one specific area, and we cannot see two types of nanostructures simultaneously. In principle, doping K plays two important roles: one is to reduce the concentration of carriers; the other method is to introduce nanopores, which is reflected by an increase in the density of the number of nanopores with the content of doping K. Volumetric sample $K_{0.02}Cu_{1.85}S$ are sufficiently dense, without visible pores. However, with an increase in the K content from x=0.01 to x=0.05, the pores appear and become more and more open. This means that the pores in bulk samples can be injected with an additional K.

The presence of nanopores in the alloy additionally reduces the thermal conductivity of the material and plays a positive role in its thermoelectric application,
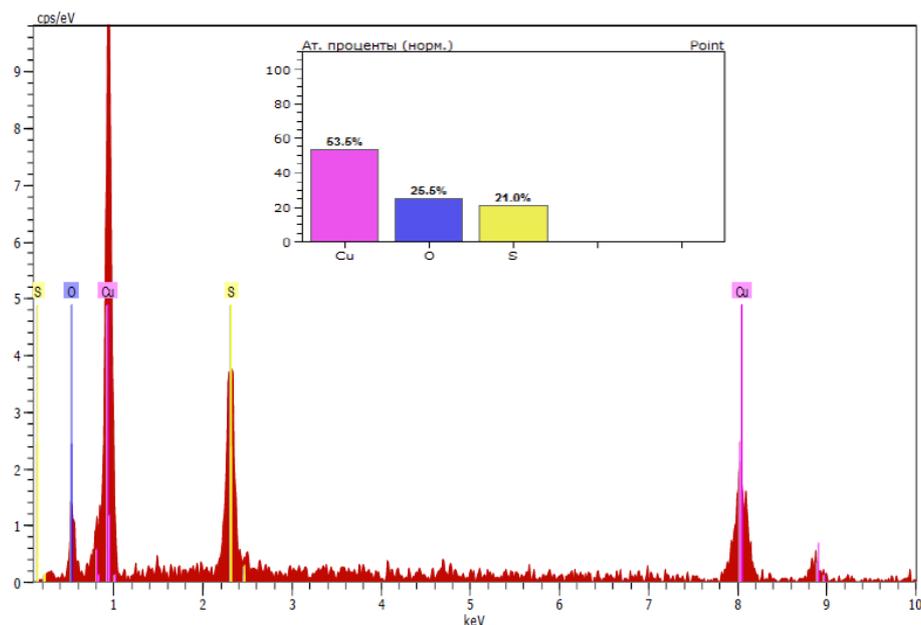
Figure 4. Calculated density of states for $K_{0.02}Cu_{1.85}S$ sample using density functional theory with Vickers hardness values for manufactured arrays.

increasing the thermoelectric figure of merit ZT of the material [11, 13, 15].

Conclusion

According to the results of X-ray phase analysis, $K_xCu_{1.85}S$ samples at room temperature consist of a mixture of various phases of copper sulfide, such as djurleite $Cu_{31}S_{16}$, chalcocite Cu_2S, roxbyite $Cu_{29}S_{16}$, anilite Cu_7S_4. Monoclinic djurleite is the prevailing phase of the alloys. All alloys contain inclusions of Cu_2O copper oxide. DTA detected a superionic phase transition from an ordered low-symmetry djurleite phase to a disordered superionic hexagonal phase of copper sulfide at about 373-383 K. Electron microscopy revealed nanopores in the $K_xCu_{1.85}S$ alloys. The mechanism of introducing nanopores using an additional K is still an open question or an unsolved problem. This can benefit from low thermal conductivity of the materials.

Acknowledgments

References

[1] P. Qiu et al., Energy Storage Materials **3** (2016) 85-97. [*CrossRef*]
[2] M. Gao et al., Chemical Society Reviews **42** (2013) 2986-3017. [*CrossRef*]
[3] F.F. Jaldurgam et al., Nanomaterials **11** (2021) 895. [*CrossRef*]
[4] Y. Sun et al., J. Mater. Chem. A. **5** (2017) 5098-5105. [*CrossRef*]

[5] M.M. Kubenova et al., Nanomaterials **11**(9) (2021) 2238. [*CrossRef*]

[6] M.Kh. Balapanov et al., Letters on materials **6**(4) (2020) 439-444. [*CrossRef*]

[7] D.J. Chakrabarti et al., Bull. Alloy Phase Diagr. **4** (1983) 254. [*CrossRef*]

[8] K. Okamoto et al., Japan. Journal of Applied Physics **12**(8) (1973) 1130-1138. [*CrossRef*]

[9] S.M. Sakhabayeva et al., Recent Contibutions to Physics. **4**(79) (2021) 72-81. [*CrossRef*]

[10] F. Gronvold et al., J. Chem. Thermodyn. **19** (1987) 1183-1198. [*CrossRef*]

[11] X. Li et al., J. Mater. Chem. A. **1** (2013) 13721-13726. [*CrossRef*]

[12] M.Kh. Balapanov et al., Vestnik Bashkirskogo universiteta **26**(4) 2021 961-964. (in Russian) [*CrossRef*]

[13] Z. Zhu et al., Appl. Phys. Mater. Sci. Process. **124** (2018) 124. [*CrossRef*]

[14] Z.H. Ge et al., Adv. Energy Mater. **6** (2016) 1600607. [*CrossRef*]

[15] Yi-xin Zhang et al., Materials Science in Semiconductor Processing **107** (2020) 104848. [*CrossRef*]

[16] W. Yong et al., Acta Phys. Sin. **62** (2013) 17802-17809. [*Google Scholar*]

[17] Y. Sumirat et al., J. Porous Mater. **13** (2006) 439. [*CrossRef*]

[18] J. Martin et al., Appl. Phys. Lett. **90** (2007) 222112. [*CrossRef*]

[19] H. Goldsmid, Materials **2** (2009) 903-910. [*CrossRef*]

[20] S.-C. Ur et al., J. Mater. Sci. **42** (2007) 2143-2149. [*CrossRef*]

[21] F.B. Swinkels et al., Acta Metall. **31** (1983) 1829-1840. [*CrossRef*]

[22] S.R. Gupta et al., Phys. Status Solidi A **8** (1971) 267-270. [*CrossRef*]

[23] P.R. Sahm, Mater. Res. Bull. **2** (1967) 85-89. [*CrossRef*]

[24] N. Savvides et al., J. Phys. C: Solid State Phys. **13** (1980) 4671. [*CrossRef*]

[25] M. Omori, Mater. Sci. Eng. A **287** (2000) 183-188. [*CrossRef*]

[26] Z. Munir et al., J. Mater. Sci. **41** (2006) 763-777. [*CrossRef*]

[27] M. Scheele et al., Adv. Funct. Mater **19** (2009) 3476. [*CrossRef*]

[28] L.D. Zhao et al., Solid State Sciences **10** (2008) 651-658. [*CrossRef*]

[29] W. Mumme et al., Can. Mineral. **50** (2012) 423-430. [*CrossRef*]

[30] M. Hellenbrandt, Crystallography Reviews **10**(1) (2004) 17-22. [*CrossRef*]

[31] K. Koto et al., Acta Crystallogr. Sect. B: Struct. Crystallogr. Cryst. Chem. **26**(7) (1970) 915-924. [*CrossRef*]

[32] R.W. Potter II, H.T. Evans Jr., J. Res. U.S. Geol. Survey **4** (1976) 205-212. [*Google Scholar*]

[33] R.J. Cava et al., Solid State Ionics. **5** (1981) 501-504. [*CrossRef*]

[34] H.T. Evans, Nature Phys. Sci. **232** (1971) 69-70. [*CrossRef*]

[35] H.T. Evans, Zeitschrift zur Kristallographie **150** (1979) 299-320. [*CrossRef*]

[36] J.B. Rivest et al., J. Phys. Chem. Lett. **2** (2011) 2402-2406. [*CrossRef*]

[37] J. Gong, P.K. Jain, Nature communications **10** (2019) 3285. [*CrossRef*]

[38] S. Parsons et al., Acta Crystallographica Section D **59** (2003) 1995-2003. [*CrossRef*]